

1 Fitness barriers limit reversion of a proofreading-deficient coronavirus

2

3 Kevin W. Graepel<sup>1,3</sup>, Maria L. Agostini<sup>1,3</sup>, Xiaotao Lu<sup>2</sup>, Nicole R. Sexton<sup>4</sup>, and Mark R.

4 Denison<sup>1,2,3#</sup>

5

6 <sup>1</sup>Department of Pathology, Microbiology, and Immunology; <sup>2</sup>Department of Pediatrics;

7 <sup>3</sup>Vanderbilt Institute for Infection, Immunology and Inflammation (VI4), Vanderbilt University

8 Medical Center, Nashville, TN, USA. <sup>4</sup>Department of Microbiology, Immunology, and

9 Pathology, College of Veterinary Medicine and Biomedical Sciences, Colorado State University,  
10 Fort Collins, CO, USA.

11

12 #Address correspondence to mark.denison@vumc.org

13

14 Running head: Barriers to reversion of a debilitated coronavirus

15

16 Keywords:

17 RNA virus, adaptive evolution, competitive fitness, coronavirus, exoribonuclease, plus-strand

18 RNA virus, proofreading, replication fidelity

19

20 Abstract word count: 359

21 Text word count: 4120

22

23 **ABSTRACT**

24 The 3'-to-5' exoribonuclease in coronavirus (CoV) nonstructural protein 14 (nsp14-ExoN)  
25 mediates RNA proofreading during genome replication. ExoN catalytic residues are arranged in  
26 three motifs: I (DE), II (E), III (D). Alanine substitution of the motif I residues (AA-E-D, four  
27 nucleotide substitutions) in murine hepatitis virus (MHV) and SARS-CoV yields viable mutants  
28 with impaired replication and fitness, increased mutation rates, and attenuated virulence *in vivo*.  
29 Despite these impairments, MHV- and SARS-CoV ExoN motif I AA mutants (ExoN-AA) have  
30 not reverted at motif I in diverse *in vitro* and *in vivo* environments, suggesting that profound  
31 fitness barriers prevent motif I reversion. To test this hypothesis, we engineered MHV-ExoN-AA  
32 with 1, 2 or 3 nucleotide mutations along genetic pathways to AA-to-DE reversion. We show  
33 that engineered intermediate revertants were viable but had no increased replication or  
34 competitive fitness compared to MHV-ExoN-AA. In contrast, a low passage (P10) MHV-ExoN-  
35 AA showed increased replication and competitive fitness without reversion of ExoN-AA.  
36 Finally, engineered reversion of ExoN-AA to ExoN-DE in the presence of ExoN-AA passage-  
37 adaptive mutations resulted in significant fitness loss. These results demonstrate that while  
38 reversion is possible, at least one alternative adaptive pathway is more rapidly advantageous than  
39 intermediate revertants and may alter the genetic background to render reversion detrimental to  
40 fitness. Our results provide an evolutionary rationale for lack of ExoN-AA reversion, illuminate  
41 potential multi-protein replicase interactions and coevolution, and support future studies aimed at  
42 stabilizing attenuated CoV ExoN-AA mutants.  
43

44 **IMPORTANCE**

45 Coronaviruses encode an exoribonuclease (ExoN) that is important for viral replication, fitness,  
46 and virulence, yet coronaviruses with a defective ExoN (ExoN-AA) have not reverted under  
47 diverse experimental conditions. In this study, we identify multiple impediments to MHV-ExoN-  
48 AA reversion. We show that ExoN-AA reversion is possible but evolutionarily unfavorable.  
49 Instead, compensatory mutations outside of ExoN-AA motif I are more accessible and beneficial  
50 than partial reversion. We also show that coevolution between replicase proteins over long-term  
51 passage partially compensates for ExoN-AA motif I but renders the virus inhospitable to a  
52 reverted ExoN. Our results reveal the evolutionary basis for the genetic stability of ExoN-  
53 inactivating mutations, illuminate complex functional and evolutionary relationships between  
54 coronavirus replicase proteins, and identify potential mechanisms for stabilization of ExoN-AA  
55 coronavirus mutants.

56 **INTRODUCTION**

57 The rapid evolution of RNA viruses represents a significant challenge for preventing, treating,  
58 and eradicating RNA viral diseases. High mutation rates in RNA viruses generate extensive  
59 opportunities to overcome evolutionary hurdles, such as antiviral drugs, host immunity, or  
60 engineered attenuating changes (1). The evolutionary pathways traversed by RNA viruses are  
61 shaped by natural selection, which will favor some evolutionary trajectories more than others  
62 based on whether mutations are beneficial, deleterious, or neutral (2). Predicting the likely results  
63 of RNA virus evolution is an important step for anticipating viral emergence and for developing  
64 escape-resistant antiviral drugs and vaccines (3, 4).

65

66 Coronaviruses (CoVs) are a family of positive-sense RNA viruses that cause human illnesses  
67 ranging from the common cold to severe and lethal respiratory disease (5). All CoVs encode a  
68 proofreading exoribonuclease within nonstructural protein 14 (nsp14-ExoN) that is critical for  
69 replication, fidelity, fitness, and virulence, and ExoN-inactivation has been proposed as a  
70 strategy for live-attenuated vaccine development (6-15). As members of the DEDDh superfamily  
71 of exonucleases, CoV ExoNs hydrolyze nucleotides using four metal-coordinating amino acids  
72 arranged in 3 motifs: I (DE), II (E), III (D) (16, 17). Alanine substitution of ExoN motif I (DE-  
73 to-AA) disrupts ExoN biochemical activity in both SARS-CoV and human CoV 229E (hCoV-  
74 229E) (16, 18, 19). The betacoronaviruses murine hepatitis virus (MHV) and SARS-CoV  
75 tolerate disruption of ExoN activity [ExoN(-)] but display mutator phenotypes accompanied by  
76 defects in replication, competitive fitness, and evasion of innate immune responses (10, 13, 14).

77 ExoN active site mutants in alphacoronaviruses, including transmissible gastroenteritis virus and  
78 hCoV-229E, have yet to be recovered and are proposed to be lethal for replication (19, 20).

79

80 Given the critical role of ExoN in CoV biology and the elevated mutation rate, we expected that  
81 natural selection would repeatedly drive reversion of the ExoN-inactivating substitutions. In line  
82 with this expectation, ExoN motif III mutants of SARS-CoV and MHV rapidly and repeatedly  
83 revert ((14) and unpublished observations). In contrast, we have never detected partial or  
84 complete reversion of ExoN motif I mutants (ExoN-AA) in SARS-CoV or MHV during 10 years  
85 of study and hundreds of experiments. More specifically, we have not detected consensus or  
86 minority variants of any kind at the motif I AA codons in either virus strain during acute  
87 infections and prolonged passage in tissue culture and following treatment with multiple  
88 nucleoside analogues (6-11, 13, 14). SARS-CoV-ExoN-AA also is stable during acute and  
89 persistent animal infections in immunocompetent and immune-compromised mice (12). The lack  
90 of primary reversion is not due simply to reduced adaptive capacity, as both SARS-CoV- and  
91 MHV-ExoN-AA can adapt for increased replication (7, 14). Most strikingly, long-term passage  
92 of MHV-ExoN-AA (250 passages, P250) yielded a highly fit population that had directly  
93 compensated for defective proofreading through evolution of a likely high-fidelity RdRp (7).  
94 Yet, where primary reversion would have required just four total consensus mutations, MHV-  
95 ExoN-AA-P250 contained more than 170.

96

97 In this study, we sought to determine whether specific genetic or fitness barriers prevent primary  
98 reversion of ExoN motif I AA. To this end, we identified and engineered viable genetic

99 pathways towards ExoN-AA motif I reversion in MHV (hereafter, ExoN-AA). Our results show  
100 that partial reversion did not confer a selective advantage compared to ExoN-AA. Further,  
101 ExoN-AA adapted within 10 passages for greater fitness than any of the intermediate revertants.  
102 Finally, restoration of WT-ExoN-DE in the setting of passage-selected mutations in the nsp12  
103 RNA-dependent RNA polymerase (RdRp) and nsp14-ExoN exacted profound fitness costs.  
104 Together, these data are the first observation of an ExoN(-) CoV genotype-fitness landscape and  
105 identify multiple genetic barriers underlying ExoN(-) motif I stability in MHV. Further, they  
106 suggest extensive coevolution between MHV replicase proteins during adaptation and reveal  
107 potential strategies for stabilizing ExoN mutant CoVs.

108

109

110 **RESULTS**

111 **Primary reversion of ExoN(-) motif I.** MHV-ExoN(-), hereafter ExoN-AA, contains two  
112 engineered substitutions in each codon of motif I, such that complete reversion to WT-ExoN-DE  
113 requires mutations to all four sites (Figure 1A). Viral mutation rates in the absence of  
114 proofreading range from  $10^{-4}$  to  $10^{-6}$  mutations per nucleotide per round of replication ( $\mu$ ) (1).  
115 Assuming an ExoN-AA mutation rate of  $10^{-4} \mu$  and accounting for codon degeneracy, the  
116 probability of restoring the native amino acid sequence in a single round of replication is  $10^{-18}$ .  
117 Only rarely do ExoN-AA titers exceed  $10^6$  PFU/mL, so it is unlikely that ExoN-AA could  
118 navigate this genetic barrier in a single infectious cycle. Thus, we hypothesized that ExoN-AA  
119 reversion, if possible, would proceed incrementally. To identify potential pathways towards  
120 ExoN-AA reversion, we examined the possible single-nucleotide substitutions surrounding A89  
121 and A91 (Figure 1B). Three mutations are synonymous, and five mutations yield amino acids  
122 unlikely to coordinate with the positively-charged metals required for ExoN catalysis (glycine,  
123 valine, proline, threonine, and serine) (16, 19, 21, 22). One mutation per site can restore the  
124 acidic charge (i.e. AA-to-ED) but not the native amino acid. These variants have not been tested  
125 in a CoV ExoN, but biochemical studies of *E. coli* DNA polymerase I ExoN mutants suggest that  
126 these conservative substitutions would not restore WT-like ExoN activity (23). We predicted  
127 stepwise pathways to ExoN-AA $\rightarrow$ DE reversion based on restoration of acidic charge followed  
128 by reversion to native amino acids (Figure 1C). We engineered and recovered variants in ExoN-  
129 AA requiring three mutations (3nt; ExoN-AD, ExoN-EA), two mutations (2nt; ExoN-DA, ExoN-  
130 ED, ExoN-AE), or one mutation (1nt; ExoN-DD, ExoN-EE) for reversion to WT-ExoN-DE  
131 (Table 1). We will hereafter refer to these mutants as intermediate revertants. All intermediate

132 revertants generated viable progeny during recovery, demonstrating that reversion to WT-ExoN-  
133 DE along these pathways is theoretically possible. The 3nt and 2nt mutants were genetically  
134 stable during recovery, as confirmed by dideoxy sequencing. However, both 1nt mutants (ExoN-  
135 DD and ExoN-EE) reverted to WT-ExoN-DE during three independent recovery attempts,  
136 suggesting that these two variants are less fit than WT-ExoN-DE and demonstrating that  
137 reversion by 1nt mutation is readily accessible. To test whether the 3nt or 2nt mutants would  
138 revert more rapidly than ExoN-AA (4nt), we passaged three lineages of each mutant 10 times at  
139 multiplicities of infection (MOI) of 0.5 and 0.01 PFU/cell. We harvested supernatants and  
140 screened for reversion by visual inspection of plaque phenotypes at each passage. WT-ExoN-DE  
141 and WT-like viruses produce uniform, large plaques, while ExoN-AA-like viruses yield small,  
142 variably-sized plaques (13). When we observed mixed plaque phenotypes, we sequenced three  
143 large plaques from each lineage to confirm reversion. The 3nt (ExoN-AD and ExoN-EA) and 2nt  
144 (ExoN-DA and ExoN-ED) intermediate revertants showed no evidence of reversion over 10  
145 passages at either MOI (Table 1). In contrast, the 2nt ExoN-AE contained WT-revertants by P2  
146 in all lineages at MOI = 0.5 PFU/cell and by P8 in one lineage at MOI = 0.01 PFU/cell. Once  
147 observed, WT-revertants dominated the ExoN-AE population for the remaining passages. These  
148 data indicate that at least one 2nt mutation pathway can lead to full reversion in tissue culture.  
149 The probability of ExoN-AE arising during a single infectious cycle of ExoN-AA is low but  
150 theoretically achievable ( $\sim 10^{-9}$ ), so ExoN-AA could conceivably revert within just two infectious  
151 cycles. However, complete reversion has never been observed even during prolonged passage or  
152 persistent infections, suggesting that additional barriers to the replication, fitness, or maintenance  
153 of intermediate revertants exist.

154 **Partial reversion of MHV-ExoN(-) motif I does not confer a selective advantage.** Because  
155 the intermediate revertants are viable as recombinants but are not found in ExoN-AA  
156 populations, we hypothesized that they confer no selective advantage over ExoN-AA (8, 9, 13).  
157 To test this hypothesis, we first analyzed replication of the 3nt and 2nt intermediate revertants  
158 (Figure 2A). All variants achieved similar peak titers to ExoN-AA, but detailed examination of  
159 their kinetics suggested a potential delay of up to 1.5 hours for all intermediate revertants  
160 compared to ExoN-AA. Of note, ExoN-AE was the most delayed, and we detected WT-ExoN-  
161 DE revertants in two of three replicates, suggesting increased selective pressure against this  
162 variant. We next measured the competitive fitness of each intermediate revertant relative to a  
163 recombinant ExoN-AA containing seven silent mutations in the nsp2 coding region (ExoN-AA-  
164 reference). Intermediate revertants were mixed with an equal titer of ExoN-AA-reference at a  
165 combined MOI = 0.05 PFU/cell and passaged four times. The ratio of each intermediate revertant  
166 to ExoN-AA-reference was quantified at each passage by RT-qPCR, and the change in ratio over  
167 time was used to calculate their relative fitness. WT-ExoN-DE was significantly more fit than  
168 ExoN-AA, whereas the intermediate revertants (ExoN-AD, -EA, -DA, and -ED) had no  
169 increased fitness relative to ExoN-AA (Figure 2B). The apparent increased fitness of ExoN-AE  
170 resulted from all lineages reverting to WT-ExoN-DE during the experiment. Finally, our  
171 previous studies have shown that adaptation of ExoN-AA includes partial compensation for the  
172 replication fidelity defect, as measured by reduced susceptibility to the mutagen 5-fluorouracil  
173 (5-FU) (7-11, 24). None of the intermediate variants demonstrated statistically significant  
174 differences in 5-FU sensitivity as compared to ExoN-AA (Figure 2C). Thus, with the exception  
175 of the ExoN-AE→DE revertants, no 3nt and 2nt intermediate genotypes along our predicted

176 pathway demonstrated an advantage in replication, fitness, or fidelity that would favor their  
177 maintenance or expansion in the viral population. Thus, natural selection is unlikely to drive  
178 ExoN-AA down these pathways towards reversion.  
179  
180 **Secondary adaptations outside of ExoN-AA motif I increase fitness along alternative**  
181 **pathways.** Although we did not find fitness advantages to intermediate revertants, we also did  
182 not identify profound fitness costs that would drive their immediate loss from populations. We  
183 have previously demonstrated that during 250 passages (P250), ExoN-AA can adapt for  
184 increased replication, fitness, and fidelity via secondary mutations outside of motif I (7). We  
185 tested whether secondary adaptive mutations could exceed the fitness of ExoN-AA and its  
186 intermediate revertants. To examine the early adaptation of ExoN-AA, we studied passage 10  
187 from the P250 passage series (Figure 3). ExoN-AA-P10 retains the ExoN-AA motif I genotype  
188 but has increased replication and reduced susceptibility to 5-FU, altogether manifesting in  
189 greater relative fitness (Figure 3) (7). We identified only six total mutations within ExoN-AA-  
190 P10 by dideoxy sequencing (Table 2), indicating that rapid adaptation of and compensation for  
191 ExoN-AA requires relatively few genetic changes at the consensus level. To test whether  
192 interactions between multiple mutations or population level effects contribute to ExoN-AA-P10  
193 fitness, we isolated a plaque-purified clone of ExoN-AA-P10. The clone replicated to higher  
194 titers than the ExoN-AA-P10 population but had identical 5-FU sensitivity and relative fitness  
195 (Figure 3), indicating that genomes derived from a single virus plaque encode the adaptive  
196 changes required by the total population. Together, these data demonstrate that mutations outside  
197 of ExoN(-) motif I can confer greater fitness advantages than intermediate revertants even at

198 early passages. These early adaptive mutations likely reduce the selective pressure for motif I  
199 reversion and place the intermediate revertants at a selective disadvantage.  
200  
201 **Adaptive mutations in nsp12 and nsp14 that increase ExoN-AA fitness confer significant**  
202 **fitness costs to WT-ExoN-DE.** Mutational fitness effects are highly dependent upon the genetic  
203 background (25-27). In addition to reducing selective pressure for reversion, mutations  
204 conferring increased fitness to ExoN-AA might also reduce the benefits of motif I reversion. We  
205 previously reported that long-term passage of ExoN-AA selects for secondary adaptive  
206 mutations in the nsp12 RdRp and nsp14 (nsp12-P250 and nsp14-P250) (7). Nsp12-P250 contains  
207 7 nonsynonymous mutations that partially compensate for defective proofreading and increase  
208 ExoN-AA fitness. Nsp14-P250 contains 6 nonsynonymous mutations, including a conservative  
209 D-to-E substitution in ExoN motif III, and increases ExoN-AA fitness without compensating for  
210 defective proofreading. To test whether the fitness effects of passage-associated mutations in  
211 nsp12-P250 and nsp14-P250 depend upon the ExoN-AA genotype, we engineered a WT motif I  
212 (ExoN-DE) into viruses containing nsp12-P250 and nsp14-P250, alone and together, and  
213 analyzed replication, 5-FU sensitivity, and competitive fitness. Compared to WT-ExoN-DE, both  
214 ExoN-DE-nsp12-P250 and ExoN-DE-nsp14-P250 displayed delayed and decreased replication  
215 (Figure 4A). In 5-FU sensitivity assays, ExoN-DE-nsp14-P250 was indistinguishable from WT-  
216 ExoN-DE, while both variants containing nsp12-P250 (ExoN-DE-nsp12-P250 and ExoN-DE-  
217 nsp12/14-P250) were significantly more sensitive to 5-FU (Figure 4B). Finally, the nsp12-P250  
218 and nsp14-P250 mutations significantly decreased fitness relative to WT-ExoN-DE (Figure 4C).  
219 We detected no statistical differences between the specific infectivity of WT-ExoN-DE and any

220 of the nsp12-P250 and nsp14-P250 variants in isolated infections (Figure 4D). Thus, mutations  
221 in nsp12 and nsp14 that arose in the ExoN-AA background were detrimental to replication,  
222 mutagen sensitivity, and competitive fitness in the presence of a fully-reverted ExoN-DE. These  
223 results support the conclusion that the adaptive pathways available to ExoN-AA may stabilize  
224 the ExoN-AA genotype, reducing both the selective pressure for, and the potential benefits of,  
225 primary reversion.

226

227 **DISCUSSION**

228 In this study, we demonstrate that the stability of the ExoN(-) motif I genotype in MHV (ExoN-  
229 AA) is a consequence of the limitations and opportunities of the genetic landscape it explores  
230 during replication (Figure 5). Our results support a model in which the viable adaptive pathways  
231 leading to direct reversion of motif I from AA-to-DE are relatively flat on a fitness landscape,  
232 with intermediate revertants remaining phenotypically ExoN(-) and conferring no fitness  
233 advantage over ExoN-AA. In contrast, at least one alternative adaptive pathway is readily  
234 accessible and imparts immediate fitness gains over ExoN-AA. We propose that even minimal  
235 alternative pathway adaptive fitness gains reduce the likelihood and benefits of motif I reversion,  
236 until eventually the changing genetic background renders reversion detrimental. These data and  
237 this model suggest that selection during replication favors immediate, incremental fitness gains  
238 along the most accessible pathway rather than dramatic fitness increases across a larger genetic  
239 barrier. While this study focused on the issue of primary ExoN-AA reversion, it raises intriguing  
240 questions about the remaining topography of the ExoN-AA fitness landscape. Ongoing studies in  
241 our laboratory will determine whether ExoN-AA-P10 (and P250) represent a conserved pathway  
242 to compensation for defective proofreading or if CoV genomes accommodate multiple solutions  
243 to ExoN(-)-associated debilitations. Supporting the possibility of limited potential pathways, a  
244 recent study of vaccine-derived polioviruses determined that evolution for virulence in parallel  
245 epidemics proceeded through a limited set of genetic changes rather than a plethora of distinct  
246 trajectories (4).

247

248 A key finding of this study is that mutations compensating for ExoN-AA are detrimental to WT-  
249 ExoN-DE, yet the mechanisms underlying this disparity are not clear. We expected that  
250 compensatory mutations in nsp14-250 would hobble WT-ExoN-DE by inducing structural  
251 changes in the active site. However, the replication and fitness defects observed in ExoN-DE  
252 viruses containing nsp14-250 were not associated with altered proofreading, as measured by 5-  
253 FU sensitivity (Figure 4). In fact, the nsp14-250 mutations do not substantially affect 5-FU  
254 sensitivity in either the ExoN-AA or WT-ExoN-DE backgrounds (7), suggesting that these  
255 mutations enhance some other stage of the MHV replication cycle, perhaps through interactions  
256 with other replicase proteins or with viral RNA. If so, these results imply that the proteins of the  
257 MHV replication holoenzyme must evolve in a highly cooperative manner to compensate for  
258 defective proofreading while also maintaining their intricate and intimate functional  
259 relationships. In line with this hypothesis, the likely high-fidelity nsp12-250 disrupted  
260 replication, 5-FU resistance, and fitness in the presence of an intact ExoN-DE catalytic motif.  
261 Given the inverse relationship between polymerase fidelity and replication speed (the slower the  
262 polymerase proceeds, the more time it has to discriminate incoming nucleotides) (28-31), nsp12-  
263 250 could fracture the delicate kinetic balance between polymerization and nsp14-ExoN-  
264 mediated excision during replication. Support for this hypothesis comes from a recent study  
265 establishing that the SARS-CoV-nsp12 replicates with lower fidelity than the RdRp of dengue  
266 virus and from the observation that the likely high-fidelity RdRp variant MHV-nsp12-V553I  
267 delays replication of proofreading-capable MHV (9, 32). As with nsp14-250, nsp12-250  
268 mutations could have additional effects on RdRp functions or protein-protein interactions that are  
269 incompatible with an active ExoN domain. Finally, it is possible that the adaptive mutations in

270 nsp12-250 and nsp14-250, including synonymous changes, could modify RNA sequence features  
271 or secondary structures in ways that interfere with WT-ExoN-DE. Defining the molecular  
272 interactions underlying the strain-specificity of ExoN-AA-compensatory mutations using  
273 recombinant viruses or reconstituted biochemical systems will provide a unique opportunity to  
274 explore the complex evolutionary and functional relationships that underpin the coronavirus  
275 replication machinery.

276

277 Our results also extend existing studies of CoV ExoN motif I. Motif I AA→DE mutations in the  
278 SARS-CoV nsp14-ExoN dramatically reduce nuclease activity in biochemical assays, but no  
279 study has examined the contributions of each residue independently (16, 18). While we cannot  
280 exclude the possibility that intermediate revertants of ExoN-AA retain some level of nucleolytic  
281 activity, the lack of consistent or statistical differences in replication, 5-FU sensitivity, or  
282 competitive fitness relative to ExoN-AA supports previous studies demonstrating that motif I DE  
283 is essential for ExoN function (16, 18, 19). Given these results, we were surprised to observe  
284 repeated reversion of the ExoN-AE but not the other two 2nt variants, ExoN-DA and ExoN-ED.  
285 One potential explanation is that the specific mutational bias of ExoN-AE makes the revertant  
286 mutations more accessible than in ExoN-DA or ExoN-ED. Alternatively, if ExoN-AE has  
287 profound replication or fitness defects, selection could drive primary reversion more quickly  
288 away from this genotype. Consistent with this hypothesis, ExoN-AE reverted more quickly at a  
289 higher MOI, where natural selection acts more efficiently on a larger population size (Table 1)  
290 (33). Biochemical studies of the ExoN-AA intermediate revertants will be valuable to determine

291 whether nsp14-ExoN-AE differs from the other intermediate revertants and to define the  
292 structural and kinetic features of nsp14-ExoN catalysis.  
293  
294 Finally, our studies suggest that compensatory mutations identified through long-term passage  
295 could be used to stabilize the ExoN-AA genotype. In particular, the high-fidelity nsp12-P250  
296 could reduce the probability of reversion by reducing mutational sampling within motif I (34),  
297 and both nsp12-P250 and nsp14-P250 render the MHV genome inhospitable to a WT-ExoN-DE.  
298 Together, these studies argue that experimental evolution can generate reagents to define critical  
299 interactions involved in CoV replication and can identify new strategies for stabilizing attenuated  
300 CoVs.  
301

302 **MATERIALS AND METHODS**

303 **Cell culture.** Delayed brain tumor (DBT-9) cells (35) and baby hamster kidney 21 cells  
304 expressing the MHV receptor (BHK-R) (36) were maintained at 37°C in Dulbecco's Modified  
305 Eagle Medium (DMEM, Gibco) supplemented with 10% serum (HyClone FetalClone II, GE  
306 Healthcare or Fetal Bovine Serum, Invitrogen), 100 U/mL penicillin and streptomycin (Gibco),  
307 and 0.25 µM amphotericin B (Corning). BHK-R cells were further supplemented with 0.8  
308 mg/mL G418 selection antibiotic (Gibco). The infectious clone of the murine hepatitis virus  
309 strain A59 (MHV-A59; GenBank accession number AY910861) was used as the template for all  
310 recombinant viruses .

311

312 **Determination of viral titer by plaque assay.** Virus samples were serially diluted and  
313 inoculated on subconfluent DBT-9 cell monolayers in either 6- or 12-well format. Cells were  
314 overlaid with 1% agar in DMEM and incubated overnight at 37°C. Plates were fixed with 4%  
315 formaldehyde and agar plugs were removed. The number of plaques per well was counted by  
316 hand and used to calculate titer (36).

317

318 **Plaque purification of viral populations.** DBT cells were infected with serial dilutions of virus  
319 and overlaid with 1% agar in DMEM. Single plaques were isolated with glass Pasteur pipettes,  
320 resuspended in PBS containing calcium and magnesium, and inoculated onto fresh DBTs. This  
321 process was completed 3 times before generating experimental stocks.

322

323 **Cloning and recovery of recombinant viruses.** Site-directed mutagenesis in MHV genome  
324 fragments was performed using “round the horn” PCR (originally described in (37)). Briefly,  
325 adjacent primers containing the mutation of interest were 5'-phosphorylated using T4  
326 polynucleotide kinase (NEB, M0201S) using the buffer from the T4 DNA ligase, which contains  
327 ATP (M0202S). PCR was performed on a plasmid template using the Q5 High-fidelity 2x  
328 Master Mix (NEB, M0492L), with primers at final concentration of 500nM. The linear  
329 amplification product was purified using the Promega Wizard SV Gel and PCR Clean-up System  
330 (Promega Corporation, A9282), and 4  $\mu$ L was ligated at 16°C overnight with the T4 DNA ligase  
331 (NEB M0202S). After transformation into chemically-competent Top10 *E. coli* (lab-derived) and  
332 expansion in liquid culture, the MHV segment of each plasmid was sequenced. Viruses were  
333 constructed, rescued, and sequenced as described previously (7, 13, 36). Experimental stocks  
334 were generated by infecting a subconfluent 150 cm<sup>2</sup> flask of DBT-9 cells at MOI of 0.01  
335 PFU/cell. Flasks were frozen at -80°C when monolayers were fully involved, approximately 20-  
336 28 hours post-infection depending on the variant. After thawing, the supernatant was clarified by  
337 centrifugation at 4,000 x g (Sorvall RC 3B Plus; HA-6000A rotor) for 10 min at 4°C. For  
338 intermediate revertants, stocks were generated in serum-free DMEM and processed as above  
339 before being concentrated roughly 10-fold by centrifugation at 4,000 x g using Amicon Ultra-15  
340 Centrifugal Filter Units, 100kDa (EMD Millipore, UFC910008). The virus titer of each stock  
341 was determined by plaque assay using DBT-9 cells as described above.

342

343 **Passage of ExoN intermediate revertants.** Intermediate revertants of ExoN-AA were passaged  
344 10 times on subconfluent DBT-9 cell monolayers in 24-well plates at an estimated MOI of either

345 0.01 or 0.5 PFU/cell. Supernatants were harvested at 24 and 20 hours post-infection for MOI =  
346 0.01 and 0.5 PFU/cell, respectively, and screened for WT reversion by plaque assay. At least  
347 three WT-like plaques were sequenced for each lineage to confirm motif I reversion.

348

349 **Replication kinetics.** Viral replication kinetics in DBT-9 cells were determined at indicated  
350 MOIs as described previously (11). Replicates were synchronized by 30-minute incubation at  
351 4°C before transferring to the 37°C incubator. Supernatant (300 µL) was harvested at the  
352 indicated time points and titered by plaque assay.

353

354 **Determination of specific infectivity.** Subconfluent monolayers of DBT-9 cells in 24-well  
355 plates were infected with the indicated virus at MOI = 0.05 PFU/cell, and supernatant was  
356 harvested at 16 hours post-infection. Genomic RNA in supernatant was quantified using one-step  
357 reverse transcription quantitative RT-PCR (RT-qPCR) on TRIzol-extracted RNA as described  
358 previously (9). Briefly, genomic RNA was detected with a 5' 6-carboxyfluorescein (FAM) and  
359 3' black hole quencher 1 (BHQ-1) labeled probe targeting nsp2 (Biosearch Technologies,  
360 Petaluma, CA), and RNA copy number was calculated by reference to an RNA standard derived  
361 from the MHV A fragment. Samples were plated in technical duplicate to minimize well-to-well  
362 variation. Titers were determined by plaque assay in DBT-9 cells, and specific infectivity was  
363 calculated as PFU per supernatant genomic RNA copy.

364

365 **5-fluorouracil sensitivity assays.** Stock solutions of 5-fluorouracil (Sigma F6627) were  
366 prepared in dimethyl sulfoxide (DMSO). Sensitivity assays were performed in 24-well plates at

367 MOI = 0.01 PFU/cell, as previously described (7). Cells were incubated with drug for 30 minutes  
368 prior to infection. Supernatants were harvested at 24 hours post-infection, and titers were  
369 determined by plaque assay.

370

371 **Competitive fitness assays.** ExoN-AA-reference and WT-ExoN-DE-reference viruses were  
372 marked with 7 consecutive silent mutations within nsp2 (wild-type: 1301-TTCGTCC-1307;  
373 reference: 1301-CAGCAGC-1307) by round the horn PCR, as described above. Competitions  
374 were performed in triplicate on DBT-9 cells in 12-well plates, plated at a density of  $1 \times 10^5$  cells  
375 per well 24 hours prior to infection. Cells were infected at a total MOI of 0.1 PFU/cell (MOI =  
376 0.05 PFU/cell each for competitor and reference virus). Supernatants were harvested 15 and 16  
377 hours post-infection for experiments with ExoN-AA-reference and WT-ExoN-DE-reference,  
378 respectively, and passaged 4 times. Samples were titered between all passages to maintain total  
379 MOI of 0.1 PFU/cell. RNA was extracted from 70  $\mu$ L of supernatant using QIAamp 96 virus  
380 QIAcube HT kit on the QIAcube HT System (Qiagen). Each RNA sample was analyzed by one-  
381 step RT-qPCR with two SYBR Green assays. Reference viruses were detected with forward  
382 primer SS-qPCR-Sil-F (5'-CTATGCTGTATACGGACAGCAGT-3'; 200nM final) and reverse  
383 primer SS-qPCR-R2 (5'-GGTGTACACCACAACAATCCAC-3', 200nM final). Competitors were  
384 detected with forward primer SS-qPCR-WT-F (5'-CTATGCT-GTATACGGATTCGTCC-3',  
385 450 nM final) and reverse primer SS-qPCR-R2 (5'-GGTGTACAC-CACAACAATCCAC-3', 450  
386 nM final). RNA samples were diluted 1:100 prior to RT-qPCR with *Power* SYBR Green RNA-  
387 to-Ct 1-step kit (Applied Biosystems) according to the manufacturer's protocol. Duplicate wells  
388 were averaged, and values were excluded from subsequent analysis if the duplicate wells differed

389 by  $> 0.5$  Ct. The relative abundance of competitor and reference were determined by subtracting  
390 Ct thresholds ( $\Delta Ct_{\text{competitor}} = Ct_{\text{competitor}} - Ct_{\text{reference}}$ ) and converted to reflect the fold-change in  
391 ratio ( $\Delta \text{ratio} = 2^{-\Delta Ct_{\text{competitor}}}$ ). The  $\log_{10}\Delta \text{ratio}$  was plotted against passage number, and the change  
392 in  $\log_{10}\Delta \text{ratio}$  (i.e. slope of linear regression) is the relative fitness. Note that regressions were fit  
393 only through P1-P4, as slight deviations in 1:1 ratio in the input (P0) can skew the slope.

394

395 **Statistical analysis.** GraphPad Prism 6 (La Jolla, CA) was used to perform statistical tests. Only  
396 the comparisons shown [e.g. ns or asterisk(s)] within the figure or legend were performed. In  
397 many cases the data were normalized to untreated controls. This was performed using GraphPad  
398 Prism 6. The number of replicate samples is denoted within each figure legend.

399

400

401

402 **ACKNOWLEDGEMENTS**

403 We thank members of the Denison laboratory and Seth Bordenstein for valuable discussions, as  
404 well as Andrea Pruijssers for critical review of the manuscript. This work was supported by  
405 United States Public Health Service awards R01-AI108197 (M.R.D), T32-GM007347 (K.W.G),  
406 F30-AI129229 (K.W.G), T32-AI089554 (N.R.S.), F31-AI133952 (M.L.A.), and T32-AI089554  
407 (M.L.A.) all from the National Institutes of Health. The content is solely the responsibility of the  
408 authors and does not necessarily represent the official views of the National Institutes of Health.  
409 The authors declare no conflicts of interest.

410

411 **REFERENCES**

- 412 1. **Sanjuán R, Nebot MR, Chirico N, Mansky LM, Belshaw R.** 2010. Viral mutation rates.  
413 *J Virol* **84**:9733–9748.
- 414 2. **Domingo E, Sheldon J, Perales C.** 2012. Viral quasispecies evolution. *Microbiol Mol*  
415 *Biol Rev* **76**:159–216.
- 416 3. **Dolan PT, Whitfield ZJ, Andino R.** 2018. Mapping the Evolutionary Potential of RNA  
417 Viruses. *Cell Host and Microbe* **23**:435–446.
- 418 4. **Stern A, Yeh Te M, Zinger T, Smith M, Wright C, Ling G, Nielsen R, Macadam A,**  
419 **Andino R.** 2017. The Evolutionary Pathway to Virulence of an RNA Virus. *Cell* **169**:35–  
420 35.e19.
- 421 5. **Perlman S, Netland J.** 2009. Coronaviruses post-SARS: update on replication and  
422 pathogenesis. *Nat Rev Microbiol* **7**:439–450.
- 423 6. **Agostini ML, Andres EL, Sims AC, Graham RL, Sheahan TP, Lu X, Smith EC, Case**  
424 **JB, Feng JY, Jordan R, Ray AS, Cihlar T, Siegel D, Mackman RL, Clarke MO,**  
425 **Baric RS, Denison MR.** 2018. Coronavirus Susceptibility to the Antiviral Remdesivir  
426 (GS-5734) Is Mediated by the Viral Polymerase and the Proofreading Exoribonuclease.  
427 *MBio* **9**:e00221–18–15.
- 428 7. **Graepel KW, Lu X, Case JB, Sexton NR, Smith EC, Denison MR.** 2017. Proofreading-  
429 Deficient Coronaviruses Adapt for Increased Fitness over Long-Term Passage without  
430 Reversion of Exoribonuclease-Inactivating Mutations. *MBio* **8**:e01503–17.

- 431 8. **Smith EC, Blanc H, Surdel MC, Vignuzzi M, Denison MR.** 2013. Coronaviruses  
432 lacking exoribonuclease activity are susceptible to lethal mutagenesis: evidence for  
433 proofreading and potential therapeutics. *PLoS Pathog* **9**:e1003565.
- 434 9. **Sexton NR, Smith EC, Blanc H, Vignuzzi M, Peersen OB, Denison MR.** 2016.  
435 Homology-Based Identification of a Mutation in the Coronavirus RNA-Dependent RNA  
436 Polymerase That Confers Resistance to Multiple Mutagens. *J Virol* **90**:7415–7428.
- 437 10. **Case JB, Li Y, Elliott R, Lu X, Graepel KW, Sexton NR, Smith EC, Weiss SR,**  
438 **Denison MR.** 2017. Murine Hepatitis Virus nsp14 Exoribonuclease Activity Is Required  
439 for Resistance to Innate Immunity. *J Virol* **92**:e01531–17–38.
- 440 11. **Smith EC, Case JB, Blanc H, Isakov O, Shomron N, Vignuzzi M, Denison MR.** 2015.  
441 Mutations in coronavirus nonstructural protein 10 decrease virus replication fidelity. *J*  
442 *Virol* **89**:6418–6426.
- 443 12. **Graham RL, Becker MM, Eckerle LD, Bolles M, Denison MR, Baric RS.** 2012. A  
444 live, impaired-fidelity coronavirus vaccine protects in an aged, immunocompromised  
445 mouse model of lethal disease. *Nat Med* **18**:1820–1826.
- 446 13. **Eckerle LD, Lu X, Sperry SM, Choi L, Denison MR.** 2007. High fidelity of murine  
447 hepatitis virus replication is decreased in nsp14 exoribonuclease mutants. *J Virol*  
448 **81**:12135–12144.
- 449 14. **Eckerle LD, Becker MM, Halpin RA, Li K, Venter E, Lu X, Scherbakova S, Graham**  
450 **RL, Baric RS, Stockwell TB, Spiro DJ, Denison MR.** 2010. Infidelity of SARS-CoV

- 451 Nsp14-exonuclease mutant virus replication is revealed by complete genome sequencing.  
452 PLoS Pathog **6**:e1000896.
- 453 15. **Menachery VD, Gralinski LE, Mitchell HD, Dinnon KH III, Leist SR, Yount BL Jr.,**  
454 **McAnarney ET, Graham RL, Waters KM, Baric RS.** 2018. Combination attenuation  
455 offers strategy for live-attenuated coronavirus vaccines. *J Virol* **JVI.00710–18–35**.
- 456 16. **Ma Y, Wu L, Shaw N, Gao Y, Wang J, Sun Y, Lou Z, Yan L, Zhang R, Rao Z.** 2015.  
457 Structural basis and functional analysis of the SARS coronavirus nsp14-nsp10 complex.  
458 *Proc Natl Acad Sci USA* **112**:9436–9441.
- 459 17. **Snijder EJ, Bredenbeek PJ, Dobbe JC, Thiel V, Ziebuhr J, Poon LLM, Guan Y,**  
460 **Rozañov M, Spaan WJM, Gorbalenya AE.** 2003. Unique and conserved features of  
461 genome and proteome of SARS-coronavirus, an early split-off from the coronavirus group  
462 2 lineage. *J Mol Biol* **331**:991–1004.
- 463 18. **Bouvet M, Imbert I, Subissi L, Gluais L, Canard B, Decroly E.** 2012. RNA 3'-end  
464 mismatch excision by the severe acute respiratory syndrome coronavirus nonstructural  
465 protein nsp10/nsp14 exoribonuclease complex. *Proc Natl Acad Sci USA* **109**:9372–9377.
- 466 19. **Minskaia E, Hertzog T, Gorbalenya AE, Campanacci V, Cambillau C, Canard B,**  
467 **Ziebuhr J.** 2006. Discovery of an RNA virus 3'→5' exoribonuclease that is critically  
468 involved in coronavirus RNA synthesis. *Proc Natl Acad Sci USA* **103**:5108–5113.

- 469 20. **Becares M, Pascual-Iglesias A, Nogales A, Sola I, Enjuanes L, Zuñiga S.** 2016.  
470 Mutagenesis of Coronavirus nsp14 Reveals Its Potential Role in Modulation of the Innate  
471 Immune Response. *J Virol* **90**:5399–5414.
- 472 21. **Steitz TA, Steitz JA.** 1993. A general two-metal-ion mechanism for catalytic RNA. *Proc*  
473 *Natl Acad Sci USA* **90**:6498–6502.
- 474 22. **Chen P, Jiang M, Hu T, Liu Q, Chen XS, Guo D.** 2007. Biochemical characterization of  
475 exoribonuclease encoded by SARS coronavirus. *J Biochem Mol Biol* **40**:649–655.
- 476 23. **Derbyshire V, Grindley ND, Joyce CM.** 1991. The 3′-5′ exonuclease of DNA  
477 polymerase I of *Escherichia coli*: contribution of each amino acid at the active site to the  
478 reaction. *EMBO J* **10**:17–24.
- 479 24. **Case JB, Ashbrook AW, Dermody TS, Denison MR.** 2016. Mutagenesis of S-  
480 Adenosyl-1-Methionine-Binding Residues in Coronavirus nsp14 N7-Methyltransferase  
481 Demonstrates Differing Requirements for Genome Translation and Resistance to Innate  
482 Immunity. *J Virol* **90**:7248–7256.
- 483 25. **Das SR, Hensley SE, Ince WL, Brooke CB, Subba A, Delboy MG, Russ G, Gibbs JS,**  
484 **Bennink JR, Yewdell JW.** 2013. Defining Influenza A Virus Hemagglutinin Antigenic  
485 Drift by Sequential Monoclonal Antibody Selection. *Cell Host and Microbe* **13**:314–323.
- 486 26. **Nakajima K, Nobusawa E, Nagy A, Nakajima S.** 2005. Accumulation of Amino Acid  
487 Substitutions Promotes Irreversible Structural Changes in the Hemagglutinin of Human  
488 Influenza AH3 Virus during Evolution. *J Virol* **79**:6472–6477.

- 489 27. **Koel BF, Burke DF, van der Vliet S, Bestebroer TM.** 2018. Epistatic interactions can  
490 moderate the antigenic effect of substitutions in hemagglutinin of influenza H3N2 virus.  
491 bioRxiv DOI 10.1101–506030.
- 492 28. **Fitzsimmons WJ, Woods RJ, McCrone JT, Woodman A, Arnold JJ, Yennawar M,**  
493 **Evans R, Cameron CE, Lauring AS.** 2018. A speed–fidelity trade-off determines the  
494 mutation rate and virulence of an RNA virus. *PLoS Biol* **16**:e2006459–20.
- 495 29. **Regoes RR, Hamblin S, Tanaka MM.** 2013. Viral mutation rates: modelling the roles of  
496 within-host viral dynamics and the trade-off between replication fidelity and speed. *Proc*  
497 *Biol Sci* **280**:20122047–20122047.
- 498 30. **Pandey VN, Kaushik N, Rege N, Sarafianos SG, Yadav PN, Modak MJ.** 1996. Role of  
499 methionine 184 of human immunodeficiency virus type-1 reverse transcriptase in the  
500 polymerase function and fidelity of DNA synthesis. *Biochemistry* **35**:2168–2179.
- 501 31. **Elena SF, Sanjuán R.** 2005. Adaptive value of high mutation rates of RNA viruses:  
502 separating causes from consequences. *J Virol* **79**:11555–11558.
- 503 32. **Ferron F, Subissi L, Silveira De Morais AT, Le NTT, Sevajol M, Gluais L, Decroly E,**  
504 **Vonrhein C, Bricogne G, Canard B, Imbert I.** 2018. Structural and molecular basis of  
505 mismatch correction and ribavirin excision from coronavirus RNA. *Proc Natl Acad Sci*  
506 *USA* **115**:E162–E171.
- 507 33. **Dolan PT, Whitfield ZJ, Andino R.** 2018. Mechanisms and Concepts in RNA Virus  
508 Population Dynamics and Evolution. *Annu Rev Virol* **5**:69–92.

- 509 34. **Arnold JJ, Vignuzzi M, Stone JK, Andino R, Cameron CE.** 2005. Remote site control  
510 of an active site fidelity checkpoint in a viral RNA-dependent RNA polymerase. *J Biol*  
511 *Chem* **280**:25706–25716.
- 512 35. **Chen W, Baric RS.** 1996. Molecular anatomy of mouse hepatitis virus persistence:  
513 coevolution of increased host cell resistance and virus virulence. *J Virol* **70**:3947–3960.
- 514 36. **Yount B, Denison MR, Weiss SR, Baric RS.** 2002. Systematic assembly of a full-length  
515 infectious cDNA of mouse hepatitis virus strain A59. *J Virol* **76**:11065–11078.
- 516 37. **Ho SN, Hunt HD, Horton RM, Pullen JK, Pease LR.** 1989. Site-directed mutagenesis  
517 by overlap extension using the polymerase chain reaction. *Gene* **77**:51–59.
- 518
- 519

520 **FIGURE LEGENDS**

521 **Figure 1. Sequence landscape around ExoN-AA motif I.** (A) ExoN motif I nucleotide sequences. (B)  
522 Landscape of single-nucleotide substitutions within ExoN-AA motif I. (C) Predicted pathways to  
523 reversion of ExoN-AA. Variants marked with # reverted to WT during three independent recovery  
524 attempts.

525

526 **Figure 2. Intermediate revertants of ExoN-AA motif I do not have selective advantages.** (A)  
527 Replication kinetics at MOI = 0.01 PFU/cell plotted as mean  $\pm$  SD of n = 3. (B) Competitive fitness of  
528 each variant relative to ExoN-AA. Viruses were competed with a tagged ExoN-AA-reference strain, and  
529 relative fitness was normalized to the mean of ExoN-AA. (C) 5-fluorouracil sensitivity at MOI = 0.01  
530 PFU/cell. Statistical significance of each variant relative to ExoN-AA was determined by one-way  
531 ANOVA with multiple comparisons (Panel D) two-way ANOVA with Dunnett's multiple comparisons  
532 (panel C). \*\*\*\*p<0.0001; ns = not significant. Data in (B) and (C) represent mean  $\pm$  SD of n = 6. Boxed  
533 values have the same significance. #All lineages of ExoN-AE reverted to WT-ExoN-DE during the  
534 experiment.

535

536 **Figure 3. ExoN-AA adapts for increased fitness within 10 passages.** (A) Replication kinetics of  
537 indicated viruses at MOI = 0.01 PFU/cell plotted as mean  $\pm$  SD of n = 3. (B) 5-fluorouracil sensitivity at  
538 MOI = 0.01 PFU/cell. (C) Competitive fitness of individual recombinants relative to ExoN-AA. Viruses  
539 were competed with a tagged ExoN-AA-reference strain, and relative fitness was normalized to the mean  
540 of ExoN-AA. Statistical significance of each virus relative to ExoN-AA was determined by two-way  
541 ANOVA with Dunnett's multiple comparisons (panel B) or by one-way ANOVA with multiple

542 comparisons (Panel C). \*\*\*\*p < 0.0001, ns = not significant. LOD = limit of detection. Data in (B) and  
543 (C) represent mean  $\pm$  SD of n = 6. Boxed values have the same significance.

544

545 **Figure 4. Mutations that increase ExoN-AA fitness are detrimental in the presence of WT-ExoN-**

546 **DE.** (A) Replication kinetics of indicated viruses at MOI = 0.01 PFU/cell plotted as mean  $\pm$  SD of n = 3.

547 (B) 5-fluorouracil sensitivity at MOI = 0.01 PFU/cell, mean  $\pm$  SD of n = 6. (C) Competitive fitness of

548 individual recombinants relative to WT-ExoN-DE. Viruses were competed with a tagged WT-ExoN-DE

549 reference strain, and relative fitness was normalized to the mean of WT-ExoN-DE, mean  $\pm$  SD of n = 6.

550 (D) Specific infectivity (genomes per PFU) from isolated infections, mean  $\pm$  SD of n = 4.. Statistical

551 significance of each virus relative to WT-ExoN-DE was determined with two-way ANOVA with

552 Dunnett's multiple comparisons test (panel B) or by ordinary one-way ANOVA with Dunnett's multiple

553 comparisons test (panels C and D). \*\*p < 0.01; \*\*\*p < 0.001; \*\*\*\*p < 0.0001; ns = not significant.

554

555 **Figure 5. Model for the *in vitro* evolution of MHV-ExoN-AA.** MHV-ExoN-AA (black dot) is a low-

556 fitness variant. Reversion to WT-ExoN-DE would dramatically increase fitness but can only be achieved

557 by traversing a flat landscape and climbing a steep fitness cliff (dotted white arrows). However,

558 secondary mutations that incrementally increase fitness are more accessible (solid white arrow).

559 Eventually, the genetic background changes enough that reversion becomes detrimental (dotted yellow

560 line).

561

562 **TABLE FOOTNOTES**

563 **Table 1. Recovery and passage of intermediate revertants.**

564 n.d.: not done.

565 <sup>a</sup>Bolded nucleotides must mutate to reach WT-ExoN-DE genotype.

566 <sup>b</sup>Recovered viruses were subjected to 10 passages at the indicated MOI. Samples were screened for wild-  
567 type revertants by plaque assay, and revertant lineages were sequence-confirmed.

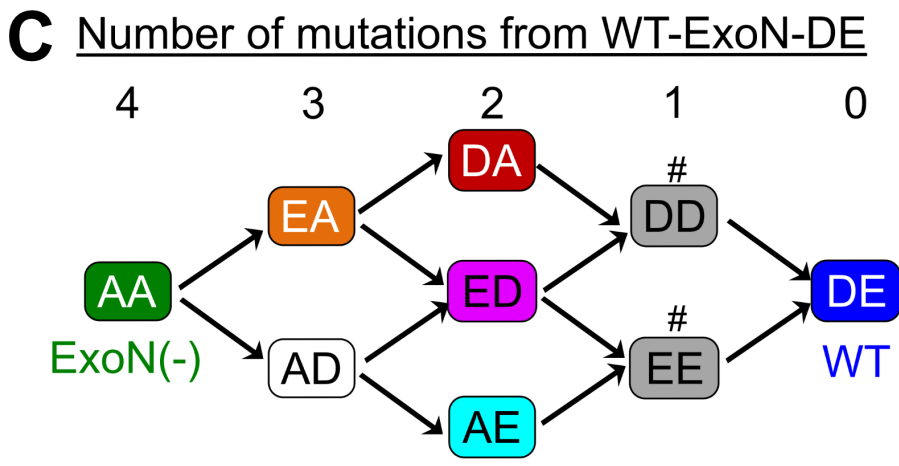
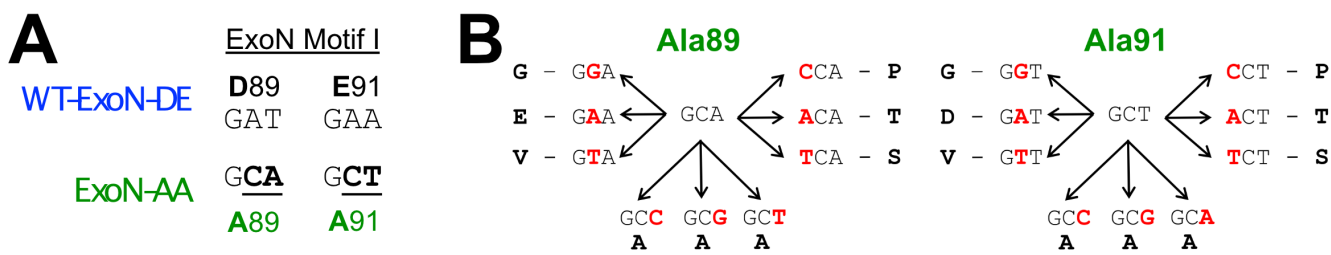
568

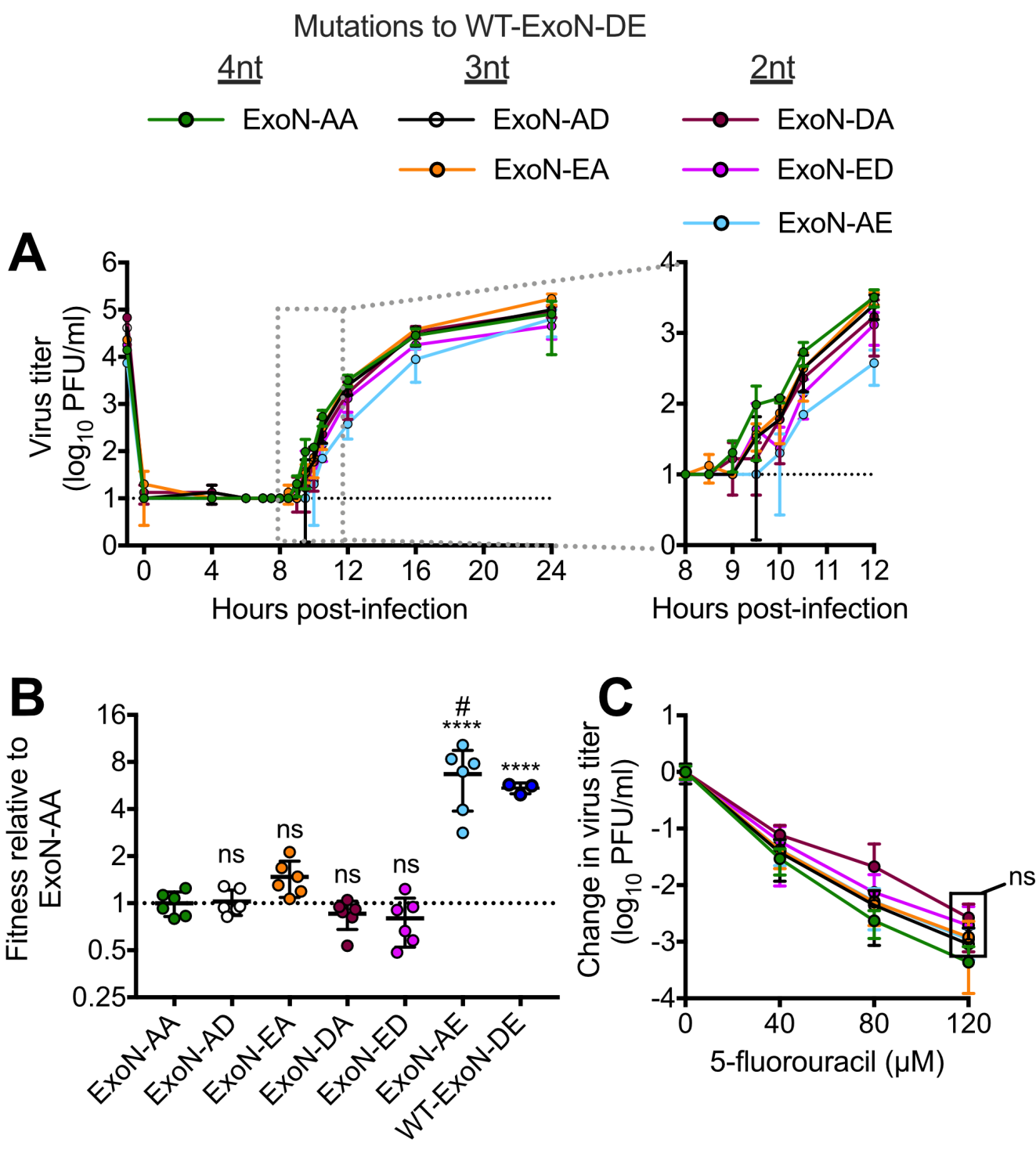
569 **Table 2. Mutations in ExoN(-) P10.** Data derived from dideoxy sequencing.

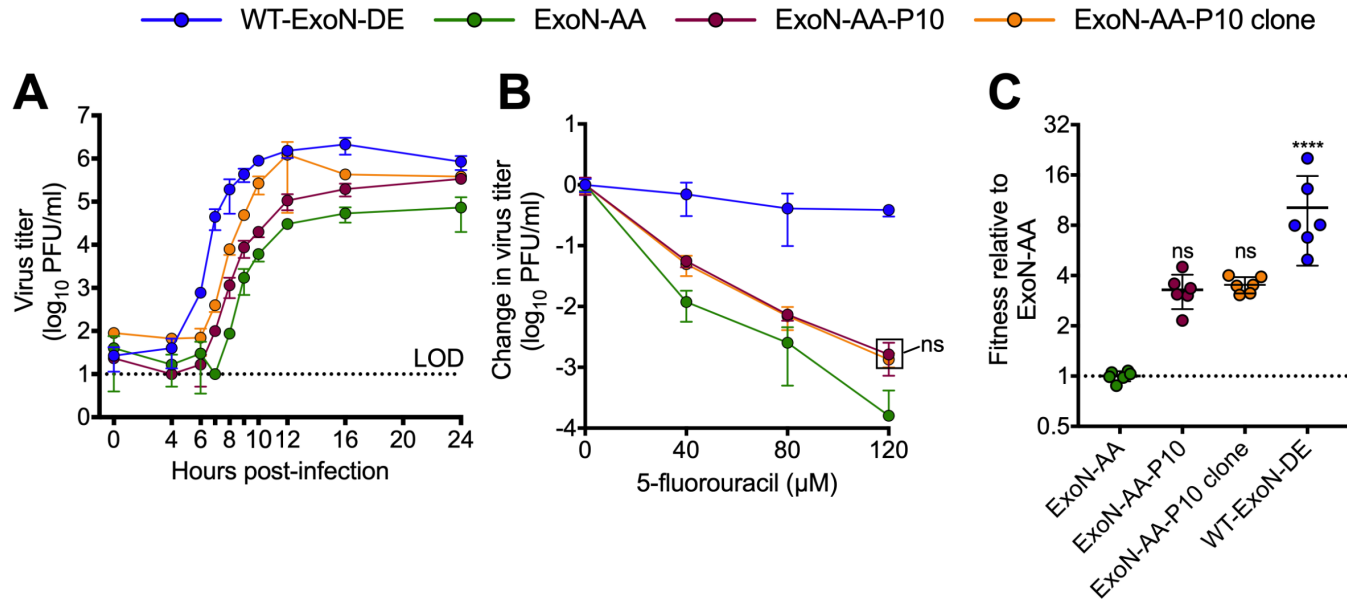
570 <sup>a</sup>Mutation present at approximately 50% of population.

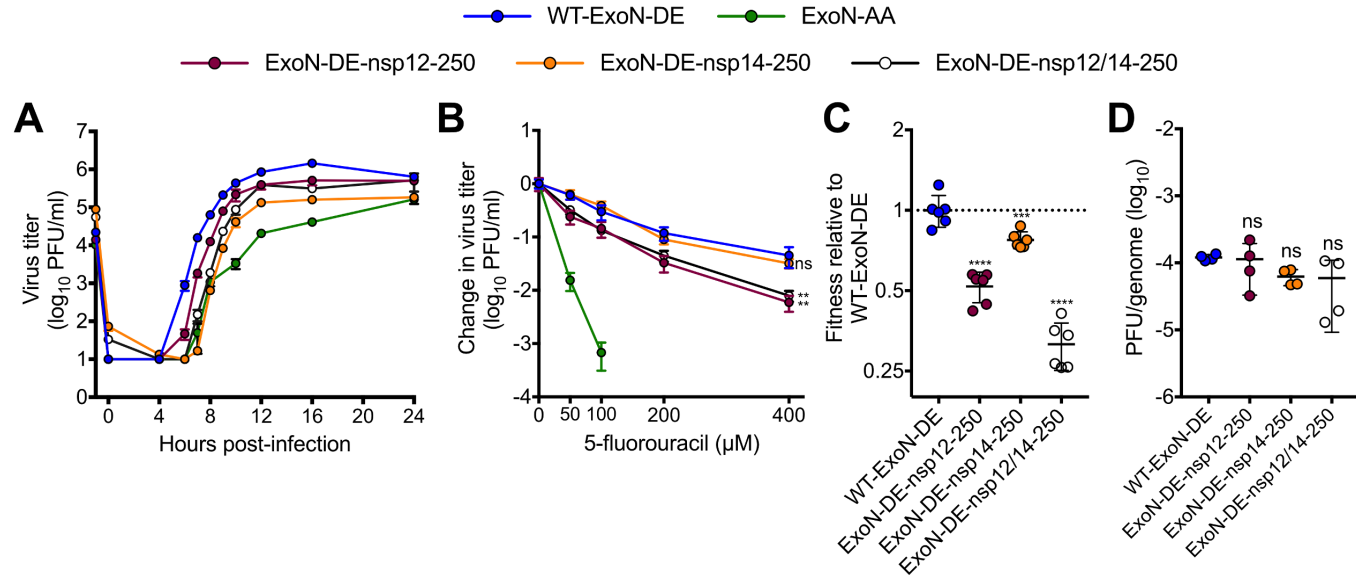
571 <sup>b</sup>MHV HE is not transcribed in tissue culture.

572 <sup>c</sup>Amino acid numbers designate positions within cleaved nsps, not the polyprotein.









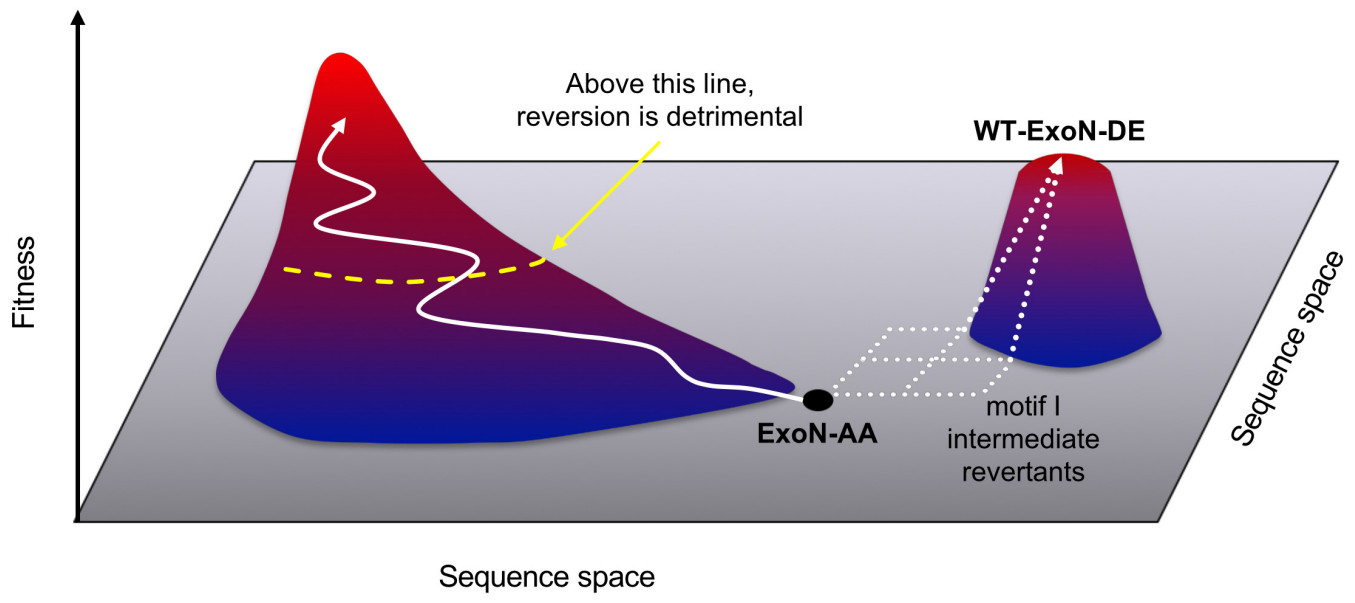


**Table 1. Recovery and passage of intermediate revertants.**

n.d.: not done.

<sup>a</sup>Bolded nucleotides must mutate to reach WT-ExoN-DE genotype.

<sup>b</sup>Recovered viruses were subjected to 10 passages at the indicated MOI. Samples were screened for wild-type revertants by plaque assay, and revertant lineages were sequence-confirmed.

Virus	# of mutations to WT-ExoN-DE	Motif I sequence <sup>a</sup>	# of reverted lineages by passage 10 <sup>b</sup>	
			MOI = 0.01	MOI = 0.5
ExoN-AA	4	<b>GCA...GCT</b>	0/3	0/3
ExoN-AD	3	<b>GCA...GAT</b>	0/3	0/3
ExoN-EA	3	<b>GAA...GCT</b>	0/3	0/3
ExoN-DA	2	<b>GAT...GCT</b>	0/3	0/3
ExoN-AE	2	<b>GCA...GAA</b>	1/3 (by P8)	3/3 (by P2)
ExoN-ED	2	<b>GAA...GAT</b>	0/3	0/3
ExoN-EE	1	<b>GAA...GAA</b>	n.d.	n.d.
ExoN-DD	1	<b>GAT...GAT</b>	n.d.	n.d.
WT-ExoN-DE	0	<b>GAT...GAA</b>	n.d.	n.d.

**Table 2. Mutations in ExoN(-) P10.** Data derived from dideoxy sequencing.

<sup>a</sup>Mutation present at approximately 50% of population.

<sup>b</sup>MHV HE is not transcribed in tissue culture.

<sup>c</sup>Amino acid numbers designate positions within cleaved nsps, not the polyprotein.

Mutation number	Nucleotide change	Protein	Amino acid change <sup>c</sup>
1	G2520A <sup>a</sup>	nsp2	D524N
2	A3080G <sup>a</sup>	nsp3	Silent
3	T16017A	nsp12	M814K
4	A17836G <sup>a</sup>	nsp13	I492M
5	G22673A <sup>a</sup>	HE <sup>b</sup>	noncoding
6	A29298C <sup>a</sup>	M	Silent